



Gutjahr, M., Ridgwell, A., Sexton, P. F., Anagnostou, E., Pearson, P. N., Pälike, H., Norris, R. D., Thomas, E., & Foster, G. L. (2017). Very large release of mostly volcanic carbon during the Palaeocene-Eocene Thermal Maximum. *Nature*, 548(7669), 573-577.  
<https://doi.org/10.1038/nature23646>

Peer reviewed version

Link to published version (if available):  
[10.1038/nature23646](https://doi.org/10.1038/nature23646)

[Link to publication record in Explore Bristol Research](#)  
PDF-document

This is the author accepted manuscript (AAM). The final published version (version of record) is available online via NATURE at <https://www.nature.com/articles/nature23646>. Please refer to any applicable terms of use of the publisher.

## University of Bristol - Explore Bristol Research

### General rights

This document is made available in accordance with publisher policies. Please cite only the published version using the reference above. Full terms of use are available:  
<http://www.bristol.ac.uk/red/research-policy/pure/user-guides/ebr-terms/>

1       **A large and mostly volcanic carbon source drove the Paleocene-**  
2                               **Eocene Thermal Maximum**

3       Marcus Gutjahr<sup>1,2\*</sup>, Andy Ridgwell<sup>3,4</sup>, Philip F. Sexton<sup>5</sup>, Eleni Anagnostou<sup>1</sup>, Paul N.  
4       Pearson<sup>6</sup>, Heiko Pälike<sup>7</sup>, Richard D. Norris<sup>8</sup>, Ellen Thomas<sup>9,10</sup> and Gavin L. Foster<sup>1</sup>

5       <sup>1</sup> Ocean and Earth Science, National Oceanography Centre Southampton, University of Southampton,  
6       UK

7       <sup>2</sup> GEOMAR Helmholtz Centre for Ocean Research Kiel, Germany [mgutjahr@geomar.de](mailto:mgutjahr@geomar.de)

8       (\* corresponding author)

9       <sup>3</sup> School of Geographical Sciences, Bristol University, Bristol, UK

10      <sup>4</sup> Department of Earth Sciences, University of California-Riverside, Riverside, CA, USA

11      <sup>5</sup> School of Environment, Earth & Ecosystem Sciences, The Open University, Milton Keynes, UK

12      <sup>6</sup> School of Earth and Ocean Sciences, Cardiff University, Cardiff, UK

13      <sup>7</sup> MARUM, Center for Marine Environmental Sciences, University of Bremen, Germany

14      <sup>8</sup> Scripps Institution of Oceanography, University of California, San Diego, La Jolla, U.S.A.

15      <sup>9</sup> Department of Geology and Geophysics, Yale University, New Haven CT, U.S.A.

16      <sup>10</sup> Department of Earth and Environmental sciences, Wesleyan University, Middletown CT, USA

Global warming during the Palaeocene-Eocene Thermal Maximum (PETM, ~56 Ma) is commonly interpreted as being driven by massive destabilization of carbon from surficial sedimentary reservoirs. If correct, this has important implications for the amplification of future fossil fuel emissions via carbon-climate feedbacks. Here we provide new paired records of boron and carbon isotope changes in the ocean that question this long-held interpretation. Our data are assimilated in an Earth system model to reconstruct the unfolding carbon cycle dynamics across the event. Strong evidence for a larger (>10,000 PgC) and on average isotopically heavier (> -17‰) carbon source leads us to identify volcanism associated with the North Atlantic Igneous Province as the main driver of the PETM. We also find that, although amplifying organic carbon feedbacks with climate likely played only a subordinate role in driving the event, enhanced organic matter burial was important in ultimately sequestering the released carbon and accelerating recovery of the Earth system.

## **Main text (2200 words)**

Aside from climate<sup>1</sup> and ecological sensitivities<sup>2</sup>, arguably the greatest uncertainties surrounding the future impact of continuing fossil fuel emissions concern the role of carbon-cycle feedbacks<sup>3,4</sup>. A past event with considerable potential to evaluate such feedbacks is the Palaeocene-Eocene Thermal Maximum (PETM)<sup>5</sup> – a 4-5°C transient surface warming<sup>6</sup> associated with ecological disruption<sup>7</sup> occurring around 55.8 million years ago<sup>8</sup>. Estimates of total carbon release vary from ~3,000 PgC to over 10,000 PgC<sup>9-12</sup>, spanning the range of present-day fossil fuel reserves<sup>13</sup> but equally reflecting considerable uncertainty in current understanding. The source(s) of carbon is also highly uncertain, and has been proposed to involve methane hydrates<sup>14</sup>, permafrost<sup>15</sup>, peatlands<sup>16</sup>, and marine sedimentary<sup>17</sup> organic matter – Earth surface carbon reservoirs that may be susceptible to modern warming and provide feedback on future climate change. Massive flood basalts and sill emplacement, associated with the North Atlantic Igneous Province (NAIP)<sup>18-21</sup>, emplaced prior to and during the PETM, represent an additional potential source of carbon, but one not linked to a feedback with climate. If we are to fully exploit the paleo-record to improve our

understanding of the longer-term consequences of anthropogenic carbon emissions, we must resolve the balance of carbon source(s) that gave rise to the PETM, and thereby deconvolve the role(s) of triggers vs. feedback. To provide new insight into the amount and source of carbon involved in PETM warming, we present new, paired, surface ocean boron (a well-established proxy for ambient surface seawater pH<sup>22</sup>) and carbon isotope data, and use these to simultaneously constrain the time-varying sources and sinks of carbon across the PETM in a novel data assimilation approach in an Earth System model (ESM).

We generated near-continuous boron, oxygen and carbon isotope records from NE Atlantic DSDP Site 401, using the surface ocean mixed-layer dwelling foraminifer *Morozovella subbotinae* (Fig. 1). We sampled the sediment sequence over an interval corresponding to ~300 ka preceding the carbon isotope excursion (CIE) to ~500 ka afterwards, using a new stratigraphy for Site 401 (Methods). To avoid alignment issues between proxies, we measured boron, oxygen and carbon isotopic compositions on the same samples (Figs. 1a, c, e and Extended Data Fig. 2).

Our measured CIE magnitude at Site 401 of -3.4‰ (Fig. 1a) is at the upper end of planktic foraminiferal  $\delta^{13}\text{C}$  records (minimum CIE: -0.7, maximum -4.4, average -2.7, n=36)<sup>5</sup>, suggesting that our sampling encompasses close to the full magnitude of the CIE (see Methods). The CIE is accompanied by a decrease in  $\delta^{11}\text{B}$  of almost 1.7‰ (Fig. 1c). The lowest  $\delta^{13}\text{C}$  and  $\delta^{11}\text{B}$  values are both observed about ~25 ka after the onset of the CIE in our preferred age model, giving an inferred duration of the onset phase of the CIE in good agreement with an independently dated record from Spitsbergen<sup>8</sup>.

Because of uncertainties in early Cenozoic seawater boron isotopic composition ( $\delta^{11}\text{B}_{\text{sw}}$ ), we tie our initial, pre-CIE boron isotope derived pH to mean ocean pH (7.75) as simulated by the ‘GENIE’ Earth System Model (ESM)<sup>23</sup> and following the approach of a previous PETM model-data pH study<sup>24</sup>. Our  $\delta^{11}\text{B}$  measurements then dictate the timing and magnitude of how ocean pH deviated from this value across the PETM. In our pH reconstruction, we calculate an uncertainty envelope accounting for uncertainties in surface ocean temperature and salinity plus  $\delta^{11}\text{B}$  measurement errors, and test two contrasting end-member  $\delta^{11}\text{B}$ -pH calibrations for the extinct foraminifer *M. subbotinae* (see Methods). We focus on the  $\delta^{11}\text{B}_{\text{foram}} = \delta^{11}\text{B}_{\text{borate}}$  calibration, giving

79 an estimated  $\delta^{11}\text{B}_{\text{SW}}$  ( $38.9 \pm 0.4\%$ ) consistent with a recent reconstruction of Eocene  
80  $\delta^{11}\text{B}_{\text{SW}}$  based on  $\delta^{11}\text{B}^{25}$ . This also gives us the most conservative possible pH  
81 excursion, as discussed below.

82 Evolution of ocean pH across the PETM is characterized by a negative  
83 excursion of 0.27 (range: 0.18-0.41) or 0.36 (0.21-0.56) pH units, depending on which  
84  $\delta^{11}\text{B}$ -pH calibration is used (Fig. 2 and Extended Data Fig. 3a, b), and in general  
85 agreement with a recently published PETM  $\delta^{11}\text{B}$  record<sup>24</sup> (Fig. 2). The wide  
86 geographic distribution, but close correspondence in magnitude of all PETM  $\delta^{11}\text{B}$ -pH  
87 records (Pacific, S. Atlantic and N. Atlantic) gives us confidence that a global surface  
88 pH excursion signal is captured at DSDP Site 401. The fact that ocean surface pH  
89 responds relatively uniformly in models<sup>2</sup> supports the evidence from multiple  $\delta^{11}\text{B}$   
90 records (Fig. 2) that a single open ocean site can be representative of the global trend  
91 (see Methods).

92 To reconstruct PETM carbon release and its average isotopic composition, we  
93 devised a novel data assimilation methodology. We build on previous work<sup>9</sup> in which  
94 a single  $\delta^{13}\text{C}$  record was assimilated ('inverted') to constrain the time-varying  
95 addition of carbon, but here exploit a more direct indicator of carbon addition – ocean  
96 surface pH (Fig. 2). This allows our  $\delta^{13}\text{C}$  record to provide a second, independent  
97 constraint on the isotopic composition of the carbon emissions in a simultaneous,  
98 transient, 500 kyr duration assimilation of both records (see Methods). We explored a  
99 wide range of different model parameterizations and proxy assumptions (Extended  
100 Data Table 1a) but focus here on the results of the data assimilation of the smoothed  
101 record.

102 From our preferred initial model configuration ('R07sm', Extended Data Table  
103 1a) we diagnose a cumulative PETM carbon release reaching  $\sim 10,200$  PgC with  
104 almost all emissions occurring in the first 50 kyr (Fig. 3d). This estimate is largely  
105 independent of the choice of age model (Extended Data Table 1), which primarily  
106 affects the cumulative carbon emissions associated with the onset interval itself (i.e.,  
107 the first trace of the CIE in our records) rather than with total emissions associated  
108 with the event as a whole. We demonstrate this in idealized model experiments in  
109 which pH and  $\delta^{13}\text{C}$  linearly decline by 0.3 pH units and 3.5‰, respectively, on time-  
110 scales ranging from 0.1 to 20 kyr (Extended Data Fig. 5 and Extended Data Table 1b).

111 We find that the total carbon emissions in our sensitivity experiments are  
112 approximately independent of the assumed duration of the onset interval (Extended  
113 Data Fig. 5 and Extended Data Table 1b), as long as the event as a whole is at least 20  
114 kyr in duration. Thus, it is the extended duration of low pH across the PETM and the  
115 existence of the co-called carbon isotope ‘plateau’<sup>6</sup> that lead to the diagnosis of  
116 emissions on the order of 10,000 PgC.

117 In response to carbon emissions, atmospheric  $p\text{CO}_2$  in the model increases from  
118  $\sim 866$  to a peak PETM value of  $2176 + 1904/-669$   $\mu\text{atm}$ , consistent with independent  
119 atmospheric  $p\text{CO}_2$  constraints based on variable terrestrial and marine  $\delta^{13}\text{C}$  gradients  
120 over the PETM<sup>26</sup>. The corresponding projected annual mean sea surface temperature  
121 (SST) increase is  $3.6^\circ\text{C}$  – close to the observation-based global mean warming  
122 estimate of  $4\text{--}5^\circ\text{C}$ <sup>6</sup>. Also in response to carbon emissions (and ocean acidification),  
123 there is a shoaling of the carbonate compensation depth (CCD) in the model – the  
124 depth horizon below which calcium carbonate ( $\text{CaCO}_3$ ) is not preserved<sup>27</sup> (Extended  
125 Data Fig. 7). In previous global carbon cycle model analyses of the PETM, the CCD  
126 has been used as a data constraint, with the conclusion that carbon emissions on the  
127 order of 10,000 PgC are too high<sup>10</sup>. In contrast, here, the relatively long ( $>50$  kyr)  
128 duration of low ocean pH conditions (Fig. 3) in conjunction with weathering  
129 feedbacks, leads to a partial decoupling of pH and ocean carbonate saturation<sup>28</sup>, hence  
130 a relatively muted response of the CCD (Extended Data Fig. 7 and Methods).

131 Diagnosed carbon emission rates peak at  $0.58 \text{ PgC yr}^{-1}$  (Fig. 3c; Extended Data  
132 Table 1a), although we assign rather less confidence to these, because their value is  
133 sensitive to the duration of the onset of the PETM and hence the specific age model  
134 (Extended Data Table 1a). To put this in perspective, for carbon input rates to  
135 approach those of current fossil fuel emissions ( $\sim 10 \text{ PgC yr}^{-1}$ <sup>13</sup>), the PETM onset  
136 would have to occur within 200–500 yr – a duration not supported by any independent  
137 age model<sup>8,9,28,29</sup>. However, we cannot rule out multiple, short-lived pulses of carbon  
138 release  $>0.58 \text{ PgC yr}^{-1}$  having occurred throughout an extended (e.g. 20 kyr) onset<sup>28</sup>.

139 In addition to the emissions diagnosed by matching the pH decline, using the  
140  $\delta^{13}\text{C}$  data as an independent constraint leads us to deduce a flux-weighted mean  $\delta^{13}\text{C}$   
141 of released carbon of  $-11\text{‰}$  (Fig. 3f, n). However, the smoothed  $\delta^{13}\text{C}$  record ( $-2.6\text{‰}$   
142 excursion) on which we focus on very likely underestimates the isotopic magnitude of

the event. For instance, assuming that the ‘true’ PETM CIE was as large as -4.0‰<sup>9,28</sup>, our mean diagnosed  $\delta^{13}\text{C}_{\text{input}}$  would become more depleted (-17‰). Uncertainty in our ocean pH reconstruction also affects the diagnosed carbon source composition. Our minimum pH decrease of 0.18 pH units requires only 5,700 PgC, with a mean  $\delta^{13}\text{C}_{\text{input}}$  that is -19‰. We note that the comparatively muted surface warming seen in this ‘minimal pH change’ model experiment (2.25°C, Extended Data Table 1a – experiment ‘R07am\_HI’) is difficult to reconcile with an observed warming of 4-5°C<sup>6</sup>. Conversely, the upper end of our measured pH increase (0.56 pH units) would require emission of considerably more carbon (19,960 PgC) with a significantly heavier carbon isotopic composition (-6.6‰) (Extended Data Table 1a).

Our diagnosed carbon input over the event likely reflects a combination of carbon source(s) – for instance, a mean of -11‰ could reflect a 75% contribution of mantle-derived carbon ( $\delta^{13}\text{C}_{\text{source}} \sim -6\text{‰}$ <sup>30</sup>) plus 25% from permafrost (-26‰<sup>31</sup>), or 90% mantle-derived plus 10% methane hydrates ( $\delta^{13}\text{C}_{\text{source}} = -60\text{‰}$ )<sup>14</sup>. In such scenarios, volcanism triggered the PETM, and thawing permafrost in Antarctica<sup>15</sup> or destabilization of methane hydrates provided amplifying feedback. Correcting for a maximum -4‰ magnitude excursion and a mean  $\delta^{13}\text{C}_{\text{input}}$  isotopically not lighter than -17‰ requires a substantial CO<sub>2</sub> contribution from volcanism<sup>20</sup>, but would allow for the possibility of a greater role for organic carbon feedbacks – almost 60% for organic matter or ~20% for methane hydrates.

To date, the PETM has predominantly been viewed as an event dominated by feedbacks between climate and reservoirs of carbon<sup>14,16</sup>, perhaps with an orbital trigger<sup>15</sup>. Yet there is abundant evidence of an intimate link in time with the opening of the North Atlantic<sup>19</sup>, with volcanism and ash deposition occurring immediately prior to PETM onset, as also recorded by declining <sup>187</sup>Os/<sup>188</sup>Os in sediments<sup>21</sup>. Radiometric dating places the PETM coincident with a ~1 Myr interval of massive flood basalt volcanism<sup>19</sup> and the emplacement of magmatic sills<sup>32</sup>, both of which represent large carbon sources. Degassing CO<sub>2</sub> from magma yields an estimated 3,600-6,000 gC m<sup>-3</sup><sup>33,34</sup> and combining this with the estimated volume of the NAIP as a whole (5×10<sup>6</sup> km<sup>3</sup> to 10×10<sup>6</sup> km<sup>3</sup><sup>19,34</sup>), gives a carbon source of 18,000-60,000 PgC. The interaction of magmatism with organic rich sediments could enhance carbon release via thermogenic methane production<sup>19,20,35,36</sup>, which is estimated to range from 3,000-6,000 PgC<sup>35,36</sup> to as high as 15,000 PgC<sup>20</sup>. Either source of carbon

176 is potentially sufficient to provide the 10,200-12,200 PgC required by our data  
177 assimilation, although our estimated mean  $\delta^{13}\text{C}_{\text{input}}$  of -11 to -17‰ would rule out  
178 either acting in isolation.

179 Our paired  $\delta^{11}\text{B}$ - $\delta^{13}\text{C}$  data also provide insights into climate system recovery  
180 from PETM warming. Once carbon emissions ceased (ca. ~55 kyr after PETM  
181 initiation – Fig. 3c), elevated global temperatures (Fig. 3a) and enhanced rates of  
182 silicate weathering (Fig. 3c) in cGENIE<sup>37</sup> (see Methods) drive a trend of increasing  
183 ocean surface pH that closely follows the observed surface ocean pH recovery (Fig.  
184 3b). However, we find a model-data misfit of up to ~1‰ in  $\delta^{13}\text{C}$  during the recovery  
185 phase (Fig. 3e). We therefore performed an additional set of experiments in which,  
186 after peak CIE, organic carbon ( $\text{C}_{\text{org}}$ ) is removed from the ocean surface<sup>38</sup> and  
187 assumed buried whenever modelled mean ocean surface  $\delta^{13}\text{C}$  registered lower values  
188 than the observed trend (see Methods). These final experiments provide close  
189 agreement with the recovery trend in the  $\delta^{13}\text{C}$  data (Fig. 3m), with cumulative  $\text{C}_{\text{org}}$   
190 burial (Fig. 3l, blue bars) of 2,500 PgC (at an average modelled marine value of -  
191 30.5‰<sup>39</sup>), in agreement with other estimates (~2,000 PgC)<sup>40</sup> of the role of enhanced  
192 organic matter burial in PETM recovery<sup>38</sup> as well as the ensuing reduction in deep-sea  
193 oxygenation<sup>41</sup>.

194 These findings collectively lead us to a view of the PETM as having been on the  
195 smaller end of a spectrum of severe perturbations of climate and carbon cycling  
196 during the Cretaceous and Jurassic (Ocean Anoxic Events – OAEs<sup>42,43</sup>), despite it  
197 having been by far the largest end-member in a series of Paleocene-Eocene  
198 ‘hyperthermal’ events<sup>44</sup>. Our pH reconstruction, in conjunction with the observed  
199  $\delta^{13}\text{C}$  decline, constrains the dominant carbon source during the PETM onset to have  
200 had a comparatively heavy carbon isotope ratio, strongly implicating volcanism as  
201 having been dominant in triggering and driving the event. Our inferred mean  $\delta^{13}\text{C}$   
202 source of -11 to -17‰ is consistent with the isotopically relatively heavy source (ca. -  
203 15‰<sup>45</sup>) inferred for the end-Permian event, suggesting mechanistic similarities  
204 between the two events<sup>34</sup>. The implied important role for organic carbon deposition in  
205 the recovery from peak warming<sup>40</sup> represents another diagnostic feature of OAEs<sup>42</sup>  
206 (and end-Permian<sup>46</sup>). Further quantifying and understanding the precise role of  
207 feedbacks – both amplifying initial  $\text{CO}_2$  release, and aiding recovery from global  
208 warming – is arguably where the PETM is of greatest value in helping reduce



209 uncertainties for our warm future. Our study, in indicating a dominant role for  
210 volcanism, points to a lower potential, at least during the prevailing warmth of the  
211 early Cenozoic, for the existence of catastrophic amplifying carbon cycle feedbacks  
212 on climate.

## 213 **Acknowledgments**

214 This study used samples provided by the International Ocean Discovery  
215 Program (IODP). We thank Andy Milton at the University of Southampton for  
216 maintaining the mass spectrometers used in this study. Lulzim Haxhijaj at GEOMAR  
217 Kiel and Henning Kuhnert at MARUM Bremen are acknowledged for their help with  
218 carbon and oxygen isotope analyses. This study was funded by UK Ocean  
219 Acidification Research Program NERC / DEFRA / DECC grant NE/H017518/1 to  
220 P.N.P., G.L.F., and P.F.S. (which supported M.G.). A.R. was supported by a Heising-  
221 Simons Foundation award, and EU grant ERC 2013-CoG-617313. ET was in part  
222 supported by NSF OCE (grant no. NSF OCE 1536611).

## 223    **References**

- 224    1       Rohling, E. J. *et al.* Making sense of palaeoclimate sensitivity. *Nature* **491**,  
225       683-691 (2012).
- 226    2       Gibbs, S. J. *et al.* Ocean warming, not acidification, controlled  
227       coccolithophore response during past greenhouse climate change. *Geology* **44**,  
228       59-62 (2016).
- 229    3       IPCC. *Climate Change 2013: The physical science basis. Contribution of*  
230       *working group I to the fifth assessment report of the intergovernmental panel*  
231       *on climate change.* (eds Stocker, T.F. *et al.*) 1-1535 (2013).
- 232    4       Hönisch, B. *et al.* The geological record of ocean acidification. *Science* **335**,  
233       1058-1063 (2012).
- 234    5       McInerney, F. A. & Wing, S. L. The Paleocene-Eocene Thermal Maximum: A  
235       perturbation of carbon cycle, climate, and biosphere with implications for the  
236       future. *Annual Review of Earth and Planetary Sciences* **39**, 489-516 (2011).
- 237    6       Dunkley Jones, T. *et al.* Climate model and proxy data constraints on ocean  
238       warming across the Paleocene-Eocene Thermal Maximum. *Earth-Science*  
239       *Reviews* **125**, 123-145 (2013).
- 240    7       Thomas, E. Cenozoic mass extinctions in the deep sea: What perturbs the  
241       largest habitat on Earth? *Geological Society of America Special Papers* **424**,  
242       1-23 (2007).
- 243    8       Charles, A. J. *et al.* Constraints on the numerical age of the Paleocene-Eocene  
244       boundary. *Geochemistry Geophysics Geosystems* **12**, Art. No. Q0AA17  
245       (2011).
- 246    9       Cui, Y. *et al.* Slow release of fossil carbon during the Palaeocene-Eocene  
247       Thermal Maximum. *Nature Geoscience* **4**, 481-485 (2011).
- 248    10       Zeebe, R. E., Zachos, J. C. & Dickens, G. R. Carbon dioxide forcing alone  
249       insufficient to explain Palaeocene-Eocene Thermal Maximum warming.  
250       *Nature Geoscience* **2**, 576-580 (2009).
- 251    11       Panchuk, K., Ridgwell, A. & Kump, L. R. Sedimentary response to Paleocene-  
252       Eocene Thermal Maximum carbon release: A model-data comparison.  
253       *Geology* **36**, 315-318 (2008).
- 254    12       Meissner, K. J. *et al.* The Paleocene-Eocene Thermal Maximum: How much  
255       carbon is enough? *Paleoceanography* **29**, 946-963 (2014).
- 256    13       Le Quéré, C. *et al.* Global Carbon Budget 2016. *Earth Syst. Sci. Data* **8**, 605-  
257       649 (2016).

- 258 14 Dickens, G. R., O'Neil, J. R., Rea, D. K. & Owen, R. M. Dissociation of  
259 oceanic methane hydrate as a cause of the carbon isotope excursion at the end  
260 of the Paleocene. *Paleoceanography* **10**, 965-971 (1995).
- 261 15 DeConto, R. M. *et al.* Past extreme warming events linked to massive carbon  
262 release from thawing permafrost. *Nature* **484**, 87-91 (2012).
- 263 16 Kurtz, A. C., Kump, L. R., Arthur, M. A., Zachos, J. C. & Paytan, A. Early  
264 Cenozoic decoupling of the global carbon and sulfur cycles.  
265 *Paleoceanography* **18**, Art. No. PA000908 (2003).
- 266 17 Higgins, J. A. & Schrag, D. P. Beyond methane: Towards a theory for the  
267 Paleocene-Eocene Thermal Maximum. *Earth and Planetary Science Letters*  
268 **245**, 523-537 (2006).
- 269 18 Eldholm, O. & Thomas, E. Environmental impact of volcanic margin  
270 formation. *Earth and Planetary Science Letters* **117**, 319-329 (1993).
- 271 19 Storey, M., Duncan, R. A. & Swisher, C. C. Paleocene-Eocene Thermal  
272 Maximum and the Opening of the Northeast Atlantic. *Science* **316**, 587-589  
273 (2007).
- 274 20 Svensen, H. *et al.* Release of methane from a volcanic basin as a mechanism  
275 for initial Eocene global warming. *Nature* **429**, 542-545 (2004).
- 276 21 Wieczorek, R., Fantle, M. S., Kump, L. R. & Ravizza, G. Geochemical  
277 evidence for volcanic activity prior to and enhanced terrestrial weathering  
278 during the Paleocene Eocene Thermal Maximum. *Geochimica et*  
279 *Cosmochimica Acta* **119**, 391-410 (2013).
- 280 22 Hönsch, B. & Hemming, N. G. Surface ocean pH response to variations in  
281  $p\text{CO}_2$  through two full glacial cycles. *Earth and Planetary Science Letters*  
282 **236**, 305-314 (2005).
- 283 23 Ridgwell, A. & Schmidt, D. N. Past constraints on the vulnerability of marine  
284 calcifiers to massive carbon dioxide release. *Nature Geoscience* **3**, 196-200  
285 (2010).
- 286 24 Penman, D. E., Hönsch, B., Zeebe, R. E., Thomas, E. & Zachos, J. C. Rapid  
287 and sustained surface ocean acidification during the Paleocene-Eocene  
288 Thermal Maximum. *Paleoceanography* **29**, 357-369 (2014).
- 289 25 Anagnostou, E. *et al.* Changing atmospheric  $\text{CO}_2$  concentration was the  
290 primary driver of early Cenozoic climate. *Nature* **533**, 380-384 (2016).
- 291 26 Schubert, B. A. & Jahren, A. H. Reconciliation of marine and terrestrial  
292 carbon isotope excursions based on changing atmospheric  $\text{CO}_2$  levels. *Nature*  
293 *Communications* **4**, Art. no. 1653 (2013).
- 294 27 Penman, D. E. *et al.* An abyssal carbonate compensation depth overshoot in  
295 the aftermath of the Palaeocene-Eocene Thermal Maximum. *Nature*  
296 *Geoscience* **9**, 575-580 (2016).

- 297 28 Turner, S. K. & Ridgwell, A. Development of a novel empirical framework  
298 for interpreting geological carbon isotope excursions, with implications for the  
299 rate of carbon injection across the PETM. *Earth and Planetary Science Letters*  
300 **435**, 1-13 (2016).
- 301 29 Röhl, U., Westerhold, T., Bralower, T. J. & Zachos, J. C. On the duration of  
302 the Paleocene-Eocene thermal maximum (PETM). *Geochemistry Geophysics*  
303 *Geosystems* **8**, Art. No. Q12002 (2007).
- 304 30 Deines, P. The carbon isotope geochemistry of mantle xenoliths. *Earth-*  
305 *Science Reviews* **58**, 247-278 (2002).
- 306 31 Dutta, K., Schuur, E. A. G., Neff, J. C. & Zimov, S. A. Potential carbon  
307 release from permafrost soils of Northeastern Siberia. *Global Change Biology*  
308 **12**, 2336-2351 (2006).
- 309 32 Svensen, H., Planke, S. & Corfu, F. Zircon dating ties NE Atlantic sill  
310 emplacement to initial Eocene global warming. *Journal of the Geological*  
311 *Society* **167**, 433-436 (2010).
- 312 33 Caldeira, K. & Rampino, M. R. The Mid-Cretaceous Super Plume, carbon  
313 dioxide, and global warming. *Geophysical Research Letters* **18**, 987-990  
314 (1991).
- 315 34 Saunders, A. D. Two LIPs and two Earth-system crises: the impact of the  
316 North Atlantic Igneous Province and the Siberian Traps on the Earth-surface  
317 carbon cycle. *Geological Magazine* **153**, 201-222 (2016).
- 318 35 Rampino, M. R. Peraluminous igneous rocks as an indicator of thermogenic  
319 methane release from the North Atlantic Volcanic Province at the time of the  
320 Paleocene–Eocene Thermal Maximum (PETM). *Bulletin of Volcanology* **75**,  
321 1-5 (2013).
- 322 36 Frieling, J. *et al.* Thermogenic methane release as a cause for the long duration  
323 of the PETM. *Proceedings of the National Academy of Sciences* **113**, 12059-  
324 12064 (2016).
- 325 37 Brady, P. V. The effect of silicate weathering on global temperature and  
326 atmospheric CO<sub>2</sub>. *Journal of Geophysical Research* **96**, 18101-18106 (1991).
- 327 38 Ma, Z. *et al.* Carbon sequestration during the Palaeocene-Eocene Thermal  
328 Maximum by an efficient biological pump. *Nature Geoscience* **7**, 382-388  
329 (2014).
- 330 39 Rau, G. H., Riebesell, U. & Wolf-Gladrow, D. A model of photosynthetic C-  
331 13 fractionation by marine phytoplankton based on diffusive molecular CO<sub>2</sub>  
332 uptake. *Marine Ecology Progress Series* **133**, 275-285 (1996).
- 333 40 Bowen, G. J. & Zachos, J. C. Rapid carbon sequestration at the termination of  
334 the Palaeocene-Eocene Thermal Maximum. *Nature Geoscience* **3**, 866-869  
335 (2010).

336 41 Pälike, C., Delaney, M. L. & Zachos, J. C. Deep-sea redox across the  
337 Paleocene-Eocene thermal maximum. *Geochemistry Geophysics Geosystems*  
338 **15**, 1038-1053 (2014).

339 42 Jenkyns, H. C. Cretaceous anoxic events - from continents to oceans. *Journal*  
340 *of the Geological Society* **137**, 171-188 (1980).

341 43 Dickson, A. J., Cohen, A. S. & Coe, A. L. Seawater oxygenation during the  
342 Paleocene-Eocene Thermal Maximum. *Geology* (2012).

343 44 Turner, S. K., Sexton, P. F., Charles, C. D. & Norris, R. D. Persistence of  
344 carbon release events through the peak of early Eocene global warmth. *Nature*  
345 *Geoscience* **7**, 748-751 (2014).

346 45 Payne, J. L. *et al.* Calcium isotope constraints on the end-Permian mass  
347 extinction. *Proceedings of the National Academy of Sciences* **107**, 8543-8548  
348 (2010).

349 46 Berner, R. A. Examination of hypotheses for the Permo-Triassic boundary  
350 extinction by carbon cycle modeling. *Proceedings of the National Academy of*  
351 *Sciences of the United States of America* **99**, 4172-4177 (2002).

## 352    **Methods**

### 353    **Site and sample selection**

354    The open northeast Atlantic DSDP Site 401 (47° 25.65' N, 08° 48.62' W, 2495 m)  
355    was selected for this study. Around 2 mg of the 250-300 µm size fraction of mixed-  
356    layer dweller *Morozovella subbotinae* were picked for the carbon, oxygen and boron  
357    isotopic analyses. Furthermore, over the studied interval, very high-resolution  $\delta^{18}\text{O}$   
358    and  $\delta^{13}\text{C}$  analyses of bulk carbonate were conducted to establish a revised age model  
359    for Site 401. Planktic foraminifera are extremely well preserved at Site 401<sup>47</sup>, free  
360    from infilling and, particularly from the onset of the CIE upwards, are semi-glassy in  
361    appearance<sup>48</sup>.

### 362    **Sample treatment**

363    Using a binocular microscope, picked foraminifera were cracked open under glass  
364    plates, the sample then homogenised, before splitting into a fraction for stable isotope  
365    ( $\delta^{18}\text{O}$  and  $\delta^{13}\text{C}$ ) analysis and another for the boron isotopic and elemental analyses  
366    (with a ratio of ca. 10:90). Purification and measurement of the boron fraction  
367    followed established protocols<sup>49,50</sup>. Samples were thoroughly cleaned to remove any  
368    adhering clays and samples were oxidatively cleaned using buffered peroxide in a  
369    warm water bath closely following<sup>51</sup>. Boron isotopic and elemental analyses were  
370    carried out on a Thermo Scientific Neptune MC-ICPMS and Element XR ICPMS,  
371    respectively, at the University of Southampton. Sample purification and handling was  
372    done in low-boron clean labs at the University of Southampton. The average boron  
373    total procedural blank was on the order of 30 to 50 pg (n>10) and is hence negligible  
374    given our typical sample size (~5 to 15 ng of B). Boron isotopic uncertainties are  
375    reported at the 2 sigma level calculated using repeats of in-house carbonate  
376    standards<sup>52</sup>. Boron isotopic and elemental aliquots were measured using additional  
377    ammonia gas for better sample washout between samples and strictly monitored  
378    during every analytical session<sup>49</sup>. Prior to analysis for boron isotopic composition,  
379    samples were screened for chemical consistency by checking various elemental ratios  
380    (B/Ca, Mg/Ca, Al/Ca etc.) (Extended Data Fig. 1). While few samples had elevated

Al/Ca (up to  $\sim 3400$   $\mu\text{mol/mol}$ ) this feature did not translate into altered  $\delta^{11}\text{B}$  (Extended Data Fig. 1).

Carbon and oxygen isotope aliquots were measured on a Thermo Finnigan MAT252 stable isotope mass spectrometer at the GEOMAR Helmholtz Centre for Ocean Research Kiel, Germany. Additionally, some foraminifera-based  $\delta^{18}\text{O}$  and  $\delta^{13}\text{C}$  analyses as well as all bulk carbonate stable isotope measurements were carried out at the MARUM Bremen, Germany on a Finnigan 251 gas isotope ratio mass spectrometer, coupled to a Kiel I automated carbonate preparation device. All produced isotope records are shown in Extended Data Fig. 2 plotted against depth in core. The carbon isotope excursion seen in our record is 3.4‰, significantly expanded relative to the benthic carbon isotope excursion presented by Nunes and Norris<sup>53</sup> that only reported an excursion on the order of 1.8‰. This discrepancy arises from the lower resolution data this earlier study<sup>53</sup> the fact that samples were not taken through the core interval of the CIE at Site 401 (202.55 to 202.41 mcd) in this earlier study. We note that Bornemann et al.<sup>47</sup> reproduced a very similar magnitude of change in  $\delta^{13}\text{C}$  to us; their  $\delta^{13}\text{C}$  data obtained from the same species (*Morozovella subbotina*) registered a shift from 4.87‰ at 202.58 mcd to 1.47‰ at 202.46 mcd (an identical excursion magnitude of 3.4‰).

### Effect of $\delta^{11}\text{B}$ -pH calibration used on resulting pH excursion

Using the appropriate  $\delta^{11}\text{B}$ -pH calibration in order to convert calcite  $\delta^{11}\text{B}$  into ambient seawater pH is essential for any paleo-pH reconstruction. For late Neogene studies using extant foraminifer species, the species used are typically calibrated for their  $\delta^{11}\text{B}_{\text{calcite}}$  to pH dependency using culture or field studies<sup>54,55</sup> in order to assess the magnitude of  $\delta^{11}\text{B}$ -vital effects that relate to foraminiferal physiology<sup>56-58</sup>. However, the species used here is extinct, making such calibrations impossible.

In order to bracket the likely magnitude of vital effects we present two calibrations, one using the  $\delta^{11}\text{B}$  to pH relationship of aqueous borate<sup>59</sup> and the other using the *T. sacculifer* calibration<sup>55</sup>. While the aqueous borate calibration is used for pH trends shown in Figs. 2 and 3, Extended Data Fig. 3a also present the alternative outcome. As noted previously<sup>24,58</sup>, when pre-PETM pH is fixed (as is the case here), the choice of  $\delta^{11}\text{B}$ -pH calibration has little impact on the reconstructed pH curve. We

note, however, that the aqueous borate calibration is more conservative and is therefore our preferred option in this case.

#### **$\delta^{18}\text{O}$ and Mg/Ca-based temperature reconstructions**

*M. subbotinae* inhabited the surface ocean mixed layer and the temperatures used for determining  $pK_B^*$  (see Extended Data Fig. 8) were determined using the  $\delta^{18}\text{O}_{\text{calcite}}$  to temperature relationship of inorganic carbonates<sup>60</sup> and a local NW Atlantic seawater  $\delta^{18}\text{O}_{\text{SMOW}}$  of 0.014‰<sup>61</sup>. Mg/Ca based temperatures shown in Extended Data Fig. 8 were calculated using deep time foraminiferal Mg/Ca paleothermometry<sup>62</sup> using identical parameters as Dunkley-Jones et al.<sup>6</sup>.

#### **Determination of $\delta^{11}\text{B}_{\text{sw}}$**

Boron in seawater has a residence time of between ~11 to 20 Ma<sup>63,64</sup> and to date the  $\delta^{11}\text{B}_{\text{sw}}$  is not well constrained for the PETM. In order to create a self-consistent model-data setup we therefore used the output of GENIE ESM in the pre-CIE configuration which for the open NE Atlantic provides a pH of 7.75<sup>23</sup>. Using this pH information and employing the generic borate ion calibration<sup>59</sup> for the pH-dependent incorporation of boron into the studied foraminifera *Morozovella subbotinae* resulted in a  $\delta^{11}\text{B}_{\text{sw}}$  of  $38.94 \pm 0.41\text{‰}$ . The uncertainty in deriving this bulk seawater  $\delta^{11}\text{B}$  is based on 10,000 realizations of a borate ion to pH conversion using the commonly used experimentally derived boron fractionation factor<sup>59</sup>, varying the given  $\delta^{11}\text{B}$  randomly within its 2 sigma measurement uncertainty, and also varying salinity by  $\pm 1.5$  psu and temperature by  $\pm 1.5^\circ\text{C}$ . Utilising the *T. sacculifer*  $\delta^{11}\text{B}$ -pH calibration<sup>55</sup>, but following the same approach, gives a  $\delta^{11}\text{B}_{\text{sw}} = 37.6 \pm 0.5\text{‰}$ .

#### **Chronology for Site 401**

A new and detailed age model was established for Site 401 by aligning our new ultra-high resolution (1 cm-spacing) bulk carbonate  $\delta^{18}\text{O}$  and  $\delta^{13}\text{C}$  records with equivalent bulk carbonate isotope records from Site 690 using the ‘Analyseries’ software<sup>65</sup>. Most stratigraphic correlation tie points (vertical lines in Extended Data Fig. 4) were made using the  $\delta^{18}\text{O}$  records, which gave excellent agreement between the sites. Site 690



currently has two detailed age models. By detailed correlations to Site 401, we were thus able to transpose both the astronomically calibrated chronology<sup>29,66</sup> and an extra-terrestrial He-based chronology<sup>67</sup> onto Site 401. Extended Data Figs. 3b and c compares our pH record from Site 401 on both chronologies.

#### **Earth system modelling – configuration and data inversion methodology**

(c)GENIE is an Earth system model of ‘intermediate complexity’ comprising: a 3-D dynamic ocean circulation model with simplified energy-moisture balance atmosphere<sup>68</sup>, a representation of the biogeochemical cycling of a variety of elements and isotopes in the ocean<sup>69</sup> including  $^{13}\text{C}$  (see ref. 70 for a summary), plus representations of the preservation and burial of biogenic carbonates in accumulating marine sediments of the open ocean<sup>70</sup>, and terrestrial weathering<sup>71,72</sup>. We utilize the cGENIE Earth system model in the same early Eocene configuration as recently employed<sup>28,73</sup> but with terrestrial weathering feedback enabled.

We introduce three separate model innovations here. The first builds on previous work<sup>9,74</sup> ‘inverting’ an observed  $\delta^{13}\text{C}$  record to recover the underlying time-history of carbon release. In this, cGENIE adjusts mean atmospheric or surface ocean  $\delta^{13}\text{C}$  to match a (proxy data) target at each time-step ( $\sim 1$  week). If the current mean model value lies *above* the data value (observed data with a coarser resolution than the model time-step is automatically linearly interpolated), a pulse of carbon is released to the atmosphere (or ocean). If the model lies *below* the data value, depending on the experimental setup, carbon is either removed from the atmosphere, or nothing is done (cf. Fig. 3). The magnitude of the carbon pulse emitted at each time-step is prescribed and chosen such that the fastest observed change in  $\delta^{13}\text{C}$  can be closely tracked, but without creating excessive overshoots in modelled  $\delta^{13}\text{C}$ . Here, we allow a maximum rate of carbon emissions to the atmosphere of  $10 \text{ PgC yr}^{-1}$  and hence a magnitude of an individual pulse of  $\sim 0.21 \text{ PgC}$ , approximately corresponding to an instantaneous increase in atmospheric  $p\text{CO}_2$  of  $0.1 \text{ ppm}$ .

We diverge from the earlier approach<sup>9,74</sup> in that rather than utilizing a record of  $\delta^{13}\text{C}$  as our model target to assimilate, we instead employ our Site 401 reconstructed surface ocean pH record. The methodology is inherently the same, but rather than comparing mean model and observed  $\delta^{13}\text{C}$  each time-step, we contrast

(model and data) pH, diagnosing the required carbon flux to the atmosphere in order that surface pH in the model tracks the data. The model-data comparison is done on the basis of a mean global surface ocean pH value calculated in cGENIE because utilizing a single (Site 401) surface ocean grid point in cGENIE creates artefacts in the diagnosed carbon emissions because there is seasonality in pH in the model but not in the data. We justify this assumption that proxy reconstructed surface ocean pH at Site 401 can be representative of the global mean, firstly on the basis of the relatively close degree of correspondence (visually) between the globally distributed pH records available, as show in Fig. 2. Secondly, ocean surface today and during the Paleocene and Eocene is relatively uniform in the model (and reality), with maximum surface gradients between upwelling regions and sub-polar regions no more than 0.1 pH units for modern, and considerably less than this in the late Paleogene (likely primarily due to the non-linear nature of the pH scale) (Extended Data Fig. 6). Furthermore, these muted patterns are retained largely unaltered in response to CO<sub>2</sub> emissions. For instance, when we calculate the annual mean surface ocean pH anomaly at different times across the PETM (experiment ID ‘R07sm\_Corg’) as compared to the pre-PETM pattern, we find a clearly generally uniform (to within  $\pm 0.02$  pH units) pattern in pH change (Extended Data Fig. 6). If we contrast the evolution of global and annual mean surface ocean pH across the PETM (‘R07sm\_Corg’) with the annual mean surface pH at the location of Site 401 for the time points available (Extended Data Fig. 6, top), we also find Site 401 pH is globally representative (and vice versa). All this goes to illustrate that there is unlikely to be any substantive artefact in our assumption of treating our pH record at Site 401 as a surrogate for the global mean in the model inversion experiment. Finally, and for comparison, a similar analysis for the modern ocean under a future ocean acidification scenario (here, chosen to follow RCP6.0) is shown in Extended Data Fig. 6 and demonstrates a similarly muted pattern of pH change.

The second innovation involves the determination of the  $\delta^{13}\text{C}$  of the carbon emitted to the atmosphere. Previously<sup>9,74</sup>, the  $\delta^{13}\text{C}$  of the carbon was treated as an unknown and a range of different possible values (and hence carbon sources and reservoirs) tested in turn. However, since observed pH constrains the magnitude of carbon emissions, we can now simultaneously employ our observed  $\delta^{13}\text{C}$  record to determine the source of carbon. The way in which the ‘double inversion’

methodology then works is that on each model time-step, following the assessment of whether or not a pulse of carbon is emitted to the atmosphere (based on the model-data pH difference), mean global model and observed Site 401  $\delta^{13}\text{C}$  values are compared. If the current mean model surface ocean  $\delta^{13}\text{C}$  value lies *above* the current data value, the carbon emitted is assigned a carbon isotopic value of -100‰. If however, the mean model value lies *below* the data value, an isotopic value of 0‰ is assigned to the carbon values. By binning the emission fluxes in time and calculating a flux-weighted average  $\delta^{13}\text{C}$ , as per in Figs. 3, intermediate (between -100 and 0 ‰)  $\delta^{13}\text{C}$  values are achieved. We emphasize that we are not assuming a source that could be -100‰ *per se*, this choice of extremely depleted value simply gives the model greater flexibility in tracking the trend in  $\delta^{13}\text{C}$ . We could have used any value just as long as it is lighter than the lightest conceivable source.

Finally, in the situation that the mean model surface ocean  $\delta^{13}\text{C}$  value becomes lower than the observed Site 401 value, we also test the importance of marine organic carbon ( $\text{C}_{\text{org}}$ ) burial. This works identically to the negative emissions diagnosed in previous studies<sup>9,74</sup> (when carbon is removed from the system to force  $\delta^{13}\text{C}$  more positive) but rather than prescribing the  $\delta^{13}\text{C}$  value, we calculate it according to a simple phytoplankton organic matter fractionation scheme<sup>69,75</sup>.

For all our experiments, we first spun up the model under late Paleocene boundary conditions<sup>28,73</sup>, here choosing an open system run time of 200 kyr in order to fully bring the long-term  $\delta^{13}\text{C}$  cycle into balance (and following on from an initially closed system spin-up of 20 kyr used to establish the basic climate and ocean circulation state). We then carried out a range of experiments as summarized in Extended Data Table 1a. We tested combinations (not all are reported here) of: (i) age model – orbital cyclostratigraphy (‘R07’) vs.  $^3\text{He}$ -based age model (‘FE’), uncertainty in the pH reconstruction – mean vs. the 2.5% and 97.5% confidence limits (‘LO’ and ‘HI’, respectively), whether or not the data is smoothed (‘sm’) or raw (‘rw’), whether or not climate-dependent weathering feedback was allowed, or weathering was fixed (‘noW’), and whether or not  $\text{C}_{\text{org}}$  burial was enabled to recover  $\delta^{13}\text{C}$  to more positive (and data tracking) values ( $\text{C}_{\text{org}}$  when carbon burial was enabled). These experiments were run for 500 kyr, with the exception of the carbon burial  $\text{C}_{\text{org}}$  series of experiments (Extended Data Table 1a), which were run for an initial interval of 72.6

kyr and up until the peak of the CIE with no organic carbon burial allowed, and then a further 227.4 kyr with carbon burial allowed when needed (for a total of 300 kyr of simulation). Model results are plotted relative to the last observed data point prior to an unambiguous onset of the CIE although in practice the cGENIE double inversion experiments were run for some ~50 kyr prior to this.

#### **Earth system modelling – additional sensitivity experiments and analysis**

We also carried out a range of sensitivity experiments to explore the importance (or otherwise) of the assumed duration of the CIE onset – in other words, whether there is a strong age model dependence of diagnosed total carbon emissions. In this series of experiments, the CIE onset phase was assumed to occur as a simultaneous linear decline in both  $\delta^{13}\text{C}$  and pH to our reconstructed peak PETM values. We varied the duration of this decline from 100 to 20,000 yr. Once the minimum in  $\delta^{13}\text{C}$  and pH was reached, these values were held constant up until the end of the experiment (a total of 50 kyr). The exact same double inversion methodology was employed. The results of these sensitivity experiments are plotted in Extended Data Fig. 5 and summarised in Extended Data Table 1b. Further details of the model and its paleo configuration, plus comprehensive discussion of model uncertainties, can be found in the supplementary information file SI 1. Additional assessments of the evolution of model-projected global mean as well as spatial patterns of sedimentary wt%  $\text{CaCO}_3$  and sea-surface temperature are illustrated in Extended Data Figs. 7 and 8, respectively (and described in SI). Site-specific model-data comparisons are shown in Extended Data Fig. 9 (and again discussed in full in SI 1).

#### **Earth system modelling – model code and supporting file availability**

The source code of the cGENIE Earth system model is available for download. Instructions regarding obtaining the model code and configuring it (and the software environment) for a range of platforms are provided via: [mycgenie.seao2.org](http://mycgenie.seao2.org). Further instructions as to how to use the model, process output etc. are also provided via a series of PDF manuals and tutorials. The specific experiment configuration files and a README describing the precise model commands needed to run these are provided under `cgenie.muffin\genie-userconfigs\MS\2017.Nature.PETM`

566 in the code tree. All other boundary conditions and data-forcing files required are  
567 automatically made available as part of the code download. The MATLAB plotting  
568 and analysis functions used are available under `cgenie.muffin\genie-matlab` in  
569 the code tree (and also automatically downloaded along with the code itself). Details  
570 of the exact parameters passed to the plotting functions and observed data plotted can  
571 be obtained directly from A.R. ([andy@seao2.org](mailto:andy@seao2.org)).

## 572    **References cited within Methods**

- 573    47    Bornemann, A. *et al.* Persistent environmental change after the Paleocene-  
574    Eocene Thermal Maximum in the eastern North Atlantic. *Earth and Planetary*  
575    *Science Letters* **394**, 70-81 (2014).
- 576    48    Sexton, P. F., Wilson, P. A. & Pearson, P. N. Microstructural and geochemical  
577    perspectives on planktic foraminiferal preservation: "Glassy" versus "Frosty".  
578    *Geochemistry Geophysics Geosystems* **7**, Art. No. Q12P19 (2006).
- 579    49    Foster, G. L. Seawater pH,  $p\text{CO}_2$  and  $[\text{CO}_3^{2-}]$  variations in the Caribbean Sea  
580    over the last 130 kyr: A boron isotope and B/Ca study of planktic foraminifera.  
581    *Earth and Planetary Science Letters* **271**, 254-266 (2008).
- 582    50    Foster, G. L. *et al.* Interlaboratory comparison of boron isotope analyses of  
583    boric acid, seawater and marine  $\text{CaCO}_3$  by MC-ICPMS and NTIMS.  
584    *Chemical Geology* **358**, 1-14 (2013).
- 585    51    Barker, S., Greaves, M. & Elderfield, H. A study of cleaning procedures used  
586    for foraminiferal Mg/Ca paleothermometry. *Geochemistry Geophysics*  
587    *Geosystems* **4**, Art. No. 8407 (2003).
- 588    52    Hennehan, M. J. *et al.* Calibration of the boron isotope proxy in the planktonic  
589    foraminifera *Globigerinoides ruber* for use in palaeo- $\text{CO}_2$  reconstruction.  
590    *Earth and Planetary Science Letters* **364**, 111-122 (2013).
- 591    53    Nunes, F. & Norris, R. D. Abrupt reversal in ocean overturning during the  
592    Palaeocene/Eocene warm period. *Nature* **439**, 60-63 (2006).
- 593    54    Sanyal, A., Bijma, J., Spero, H. & Lea, D. W. Empirical relationship between  
594    pH and the boron isotopic composition of *Globigerinoides sacculifer*:  
595    Implications for the boron isotope paleo-pH proxy. *Paleoceanography* **16**,  
596    515-519 (2001).
- 597    55    Martinez-Boti, M. A. *et al.* Boron isotope evidence for oceanic carbon dioxide  
598    leakage during the last deglaciation. *Nature* **518**, 219-222 (2015).
- 599    56    Zeebe, R. E., Wolf-Gladrow, D. A., Bijma, J. & Honisch, B. Vital effects in  
600    foraminifera do not compromise the use of delta B-11 as a paleo-pH indicator:  
601    Evidence from modeling. *Paleoceanography* **18**, Art. No. 1043 (2003).
- 602    57    Honisch, B. *et al.* The influence of symbiont photosynthesis on the boron  
603    isotopic composition of foraminifera shells. *Marine Micropaleontology* **49**,  
604    87-96 (2003).
- 605    58    Foster, G. L. & Rae, J. W. B. Reconstructing ocean pH with boron isotopes in  
606    foraminifera. *Annual Review of Earth and Planetary Sciences* **44**, 207-237  
607    (2016).

- 608 59 Klochko, K., Kaufman, A. J., Yao, W. S., Byrne, R. H. & Tossell, J. A.  
609 Experimental measurement of boron isotope fractionation in seawater. *Earth*  
610 *and Planetary Science Letters* **248**, 276-285 (2006).
- 611 60 Kim, S.-T. & O'Neil, J. R. Equilibrium and nonequilibrium oxygen isotope  
612 effects in synthetic carbonates. *Geochimica et Cosmochimica Acta* **61**, 3461-  
613 3475 (1997).
- 614 61 Tindall, J. *et al.* Modelling the oxygen isotope distribution of ancient seawater  
615 using a coupled ocean-atmosphere GCM: Implications for reconstructing early  
616 Eocene climate. *Earth and Planetary Science Letters* **292**, 265-273 (2010).
- 617 62 Evans, D. & Müller, W. Deep time foraminifera Mg/Ca paleothermometry:  
618 Nonlinear correction for secular change in seawater Mg/Ca.  
619 *Paleoceanography* **27**, Art. No. PA4205 (2012).
- 620 63 Spivack, A. J. & Edmond, J. M. Boron isotope exchange between seawater  
621 and the oceanic crust. *Geochimica et Cosmochimica Acta* **51**, 1033-1043  
622 (1987).
- 623 64 Lemarchand, D., Gaillardet, J., Lewin, E. & Allegre, C. J. Boron isotope  
624 systematics in large rivers: implications for the marine boron budget and  
625 paleo-pH reconstruction over the Cenozoic. *Chemical Geology* **190**, 123-140  
626 (2002).
- 627 65 Paillard, D., Labeyrie, L. & Yiou, P. Macintosh program performs time -  
628 series analysis. *Eos, Transactions American Geophysical Union* **77**, 379-379  
629 (1996).
- 630 66 Röhl, U., Bralower, T. J., Norris, R. D. & Wefer, G. New chronology for the  
631 late Paleocene thermal maximum and its environmental implications. *Geology*  
632 **28**, 927-930 (2000).
- 633 67 Farley, K. A. & Eltgroth, S. F. An alternative age model for the Paleocene-  
634 Eocene Thermal Maximum using extraterrestrial He-3. *Earth and Planetary*  
635 *Science Letters* **208**, 135-148 (2003).
- 636 68 Edwards, N. R. & Marsh, R. Uncertainties due to transport-parameter  
637 sensitivity in an efficient 3-D ocean-climate model. *Clim Dyn* **24**, 415-433  
638 (2005).
- 639 69 Ridgwell, A. *et al.* Marine geochemical data assimilation in an efficient Earth  
640 System Model of global biogeochemical cycling. *Biogeosciences* **4**, 87-104  
641 (2007).
- 642 70 Ridgwell, A. & Hargreaves, J. C. Regulation of atmospheric CO<sub>2</sub> by deep-sea  
643 sediments in an Earth system model. *Glob. Biogeochem. Cycle* **21**, Art. No.  
644 GB2008 (2007).
- 645 71 Colbourn, G., Ridgwell, A. & Lenton, T. M. The time scale of the silicate  
646 weathering negative feedback on atmospheric CO<sub>2</sub>. *Glob. Biogeochem. Cycle*  
647 **29**, 583-596 (2015).

- 648 72 Lord, N. S., Ridgwell, A., Thorne, M. C. & Lunt, D. J. The ‘long tail’ of  
649 anthropogenic CO<sub>2</sub> decline in the atmosphere and its consequences for post-  
650 closure performance assessments for disposal of radioactive wastes.  
651 *Mineralogical Magazine* **79**, 1613-1623 (2015).
- 652 73 Zeebe, R. E., Ridgwell, A. & Zachos, J. C. Anthropogenic carbon release rate  
653 unprecedented during the past 66 million years. *Nature Geoscience* **9**, 325–  
654 329 (2016).
- 655 74 Cui, Y. & Kump, L. R. Global warming and the end-Permian extinction event:  
656 Proxy and modeling perspectives. *Earth-Science Reviews* **149**, 5-22 (2015).
- 657 75 Ridgwell, A. *Glacial-interglacial perturbations in the global carbon cycle*  
658 PhD thesis, Univ. of East Anglia at Norwich, UK, (2001).
- 659 76 Cao, L. *et al.* The role of ocean transport in the uptake of anthropogenic CO<sub>2</sub>.  
660 *Biogeosciences* **6**, 375-390 (2009).



661 **Manuscript Figure Captions**

662 **Fig. 1.** Foraminifera (*M. subbotinae*) (a) and bulk carbonate  $\delta^{13}\text{C}$  (b),  $\delta^{11}\text{B}$  (c) and  
663  $\delta^{18}\text{O}$  (d and e) records plotted relative to the onset of the PETM carbon isotope  
664 excursion (CIE) from DSDP Site 401 (47° 25.65' N, 08° 48.62' W, 2495 m) using our  
665 preferred age model (see Methods).

666 **Fig. 2.** *M. subbotinae* based  $\delta^{13}\text{C}$  and boron isotope based pH reconstructions of Site  
667 401. Panels A and B show the entire record, while C and D focus on the CIE interval.  
668 Also shown are data of ref. 24 on the original age model with pH values recalculated  
669 using a laboratory offset such that pre-PETM pH calculated using our Monte Carlo  
670 approach at Site 1209 = 7.74 given the distribution of seawater  $\delta^{11}\text{B}$  determined at  
671 Site 401 ( $38.9 \pm 0.4\text{‰}$ ). This resulted in a mean correction of the literature data<sup>24</sup> of -  
672 0.32‰.

673 **Fig. 3.** Output of the GENIE ESM data assimilation experiment in which both  $\delta^{13}\text{C}$   
674 and pH records were simultaneously inverted. The left hand panels show the results of  
675 the first series of data assimilation in which no organic carbon burial was allowed (i.e.  
676 positive carbon input to the ocean and atmosphere only) and are as follows: (a) Model  
677 diagnosed trajectories of atmospheric  $p\text{CO}_2$  (red, LH axis) and mean global SST  
678 (blue, RH axis), with the mean trajectory in bold and the 95% uncertainty limits as a  
679 shaded band. (b) Interpolated surface ocean pH data (yellow symbols) together with  
680 model trajectories of mean global ocean surface pH, with the mean trajectory in bold  
681 and the 95% uncertainty limits as a shaded band. (c) Model diagnosed rates of  $\text{CO}_2$   
682 release to the atmosphere in 2 kyr bins. The central estimate (red) is show together  
683 with 95% uncertainty limits (empty bars). Rates of excess  $\text{CO}_2$  due to silicate  
684 weathering is shown in green. (d) Cumulative  $\text{CO}_2$  release to the atmosphere in 2 kyr  
685 bins. The central estimate (red) is show together with 95% uncertainty limits (empty  
686 bars). (e) Interpolated surface ocean  $\delta^{13}\text{C}$  data (yellow symbols) together with model  
687 trajectories of mean global ocean surface  $\delta^{13}\text{C}$ , with the mean trajectory in bold and  
688 the 95% (pH-derived) uncertainty limits as a shaded band. (f) Model diagnosed  $\delta^{13}\text{C}$   
689 of the  $\text{CO}_2$  release. The central estimate (red) is show together with 95% uncertainty  
690 limits (empty bars). The right hand panels show the results of the second series of

691 data assimilation in which organic carbon burial was allowed. The panels are as per a-  
692 f with the exception of: (k), which shows the diagnosed rates of organic carbon burial  
693 (blue), (l), cumulative organic carbon burial (blue), and (n), the isotopic composition  
694 of burial carbon (blue). All experiments assumed and are plotted along with the data  
695 on our preferred orbital age model<sup>29</sup> and are plotted from -50 to +150 kyr relatively to  
696 the onset of the CIE.

697 **Extended Data Figure Captions**

698

699 **Extended Data Fig. 1.** Elemental and stable isotope cross-plots for *M. subbotinae*  
700 measured in this study.

701 **Extended Data Fig. 2.** Foraminifera- and bulk carbonate  $\delta^{13}\text{C}$ ,  $\delta^{18}\text{O}$  and  $\delta^{11}\text{B}$  data  
702 plotted against depth in core. Foraminifera-based stable isotope compositions were  
703 generated from identical samples after splitting of  $\delta^{13}\text{C}$  /  $\delta^{18}\text{O}$  fraction from  $\delta^{11}\text{B}$   
704  $^{67}$ fraction.

705 **Extended Data Fig. 3.** (a) Comparison of pH evolution at Site 401 over the PETM  
706 CIE using either the borate ion (red) or alternatively the *T. sacculifer* (green)  
707 calibration. Age scale used is following Röhl et al.<sup>29</sup>. (b) Direct comparison of our  
708 two age models, showing the reconstructed pH evolution of Site 401 plotted using  
709 either the age model of Farley and Eltgroth<sup>67</sup> or our preferred age model of Röhl et  
710 al.<sup>29</sup>. (c) Expanded view of (b).

711 **Extended Data Fig. 4.** Bulk carbonate  $\delta^{13}\text{C}$  and  $\delta^{18}\text{O}$  comparison between Site 401  
712 and Site 690 presented in Röhl et al.<sup>29</sup>. Vertical lines highlight age tie points used to  
713 derive the age model relative to the PETM carbon isotope excursion.

714 **Extended Data Fig. 5.** Sensitivity experiments illustrating the importance of  
715 uncertainties in the age model for the CIE onset. In these experiments, the CIE onset  
716 phase is assumed to occur linearly, with a duration of the decline in  $\delta^{13}\text{C}$  and pH that  
717 varies from 100 to 20,000 yr duration, with the target pH and  $\delta^{13}\text{C}$  values thereafter  
718 held constant until the end of the experiment (50,000 yr). The evolution with time of  
719 these target ocean surface variables is shown in the uppermost panels (a), with pH on  
720 the left hand y-axis, and  $\delta^{13}\text{C}$  on the right hand y-axis. The lower rows of panels  
721 show: (b) maximum emission rate per time interval, (c) cumulative carbon emission  
722 for respective onset phase in EgC (1 Eg =  $10^{18}$  g) and (d) average emitted  $\delta^{13}\text{C}$  per  
723 time interval. Results shown with onset phases ranging from 100 years to a maximum  
724 of 20 ka.

**Extended Data Fig. 6.** Illustration of the spatial and temporal evolution of mean annual surface ocean pH in the cGENIE Earth system model both across the PETM and for illustration, the modern mean annual surface ocean pH projected from the preindustrial and into the future under RCP 6.0<sup>3</sup>. Shown are: (a) Global and annual mean surface ocean pH (black solid line) across the PETM from experiment ‘R07sm\_Corg’ (our central pH estimate, using the inorganic borate ion calibration and the RH07 age model, and including an assumption of organic carbon burial post peak PETM). Red circles represent the annual mean pH values at the location of Site 401 in the model (see location in panel b) at the times from PETM onset onwards that corresponding to the  $\delta^{11}\text{B}$  derived pH data points (cf. Fig. 3b). (b) Model projected spatial pattern of annual mean surface ocean pH at time zero (i.e. PETM onset). (c-f) Model projected spatial pattern of the annual mean surface ocean pH anomaly compared to time zero, for the highlighted time-points in (a) – 5.0, 31.6, 58.2, and 71.5 kyr following onset. (g) Model projected spatial pattern of annual mean surface ocean pH in the modern ocean under pre-industrial atmospheric CO<sub>2</sub> (278 ppm). The model is configured as per described in *Cao et al.*<sup>76</sup> and driven with a CO<sub>2</sub> scenario calculated consistent with RCP 6.0. The scale is chosen to be the same as per (b). (h-i) Model projected spatial pattern of the annual mean surface ocean pH anomaly compared to 1765, at year 2010 and 2050. The scale is chosen to be the same as per (c-f).

**Extended Data Fig. 7.** Illustration of the spatial and temporal evolution of surface sedimentary carbonate content in the cGENIE Earth system model across the PETM. Shown are: (a) Global mean surface sedimentary wt% CaCO<sub>3</sub> (black solid line) across the PETM from experiment ‘R07sm\_Corg’. White circles represent the times from PETM onset onwards that correspond to the  $\delta^{11}\text{B}$  derived pH data points as per in Fig. 3b and Extended Data Fig. 6. Note that the white circles do not represent ‘values’ and are plotted simply as markers of specific time-points. (b) Model projected spatial pattern of surface sedimentary wt% CaCO<sub>3</sub> at time zero (i.e. PETM onset). Shown are the locations of sites for which surface ocean pH has been reconstructed (see Fig. 2) and at which detailed down-core model-data comparison is carried out (Extended Data Fig. 9). (c-f) Model projected spatial pattern of the surface sedimentary wt% CaCO<sub>3</sub> anomaly compared to time zero, for the highlighted time-points in (a) – 5.0,

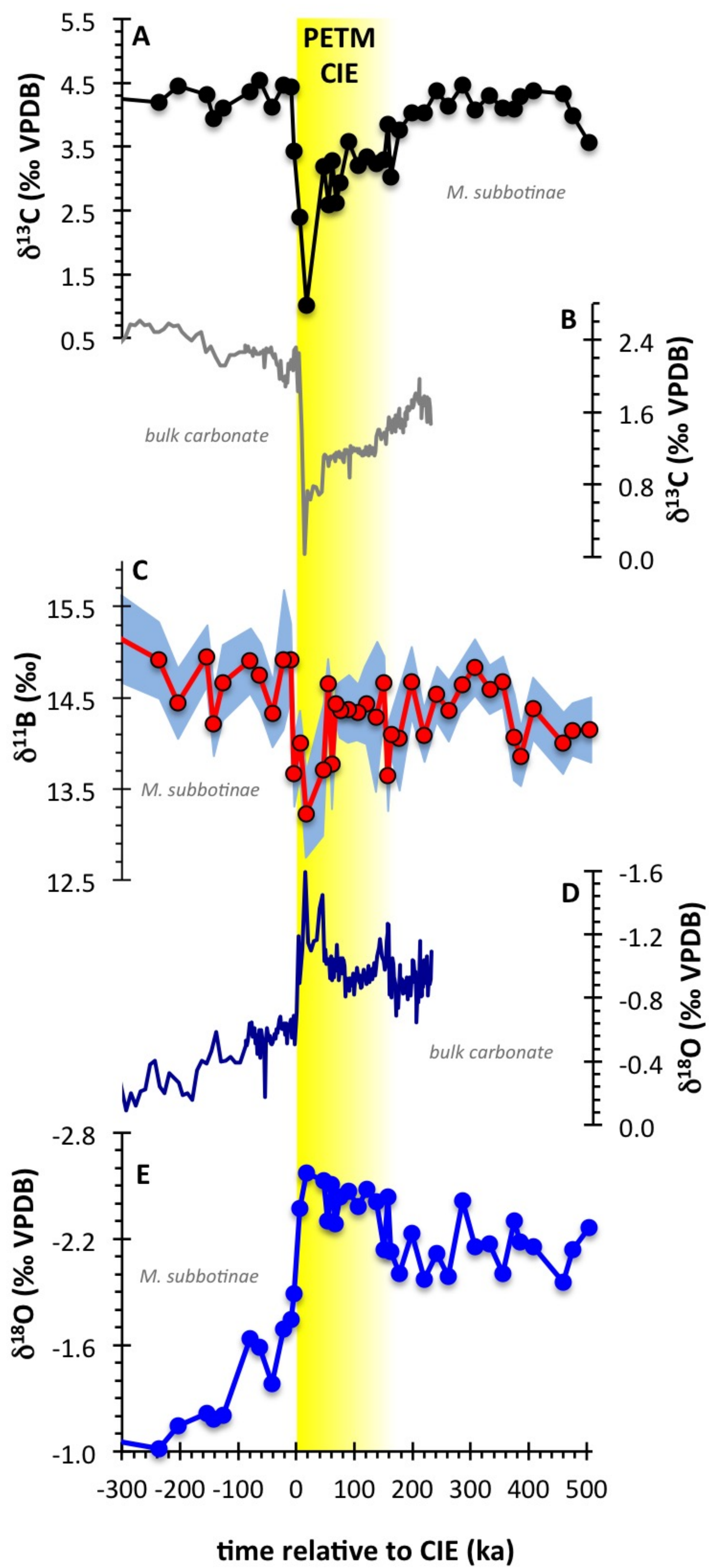
31.6, 58.2, and 71.5 kyr following onset. (g) For reference – the assumed seafloor bathymetry in the model (together with the four data-rich sites focussed on in the SI analysis).

**Extended Data Fig. 8.** Illustration of the spatial and temporal evolution of sea surface temperature in the cGENIE Earth system model across the PETM. Shown are: (a) Global and annual mean sea surface temperature (SST) (black solid line) across the PETM from experiment ‘R07sm\_Corg’. Yellow circles represent the annual mean SST values at the location of Site 401 in the model at the times from PETM onset onwards that corresponding to the  $\delta^{11}\text{B}$  derived pH data points (cf. Fig. 3b). Orange and blue filled circles represent Mg/Ca and  $\delta^{18}\text{O}$  derived, respectively, SST estimates. (b) Model projected spatial pattern of annual mean SST at time zero. The location of Site 401 in the model is highlighted by a star. (c-f) Model projected spatial pattern of the annual mean SST anomaly compared to time zero, for the highlighted time-points in (a) (yellow circles) – 5.0, 31.6, 58.2, and 71.5 kyr following onset.

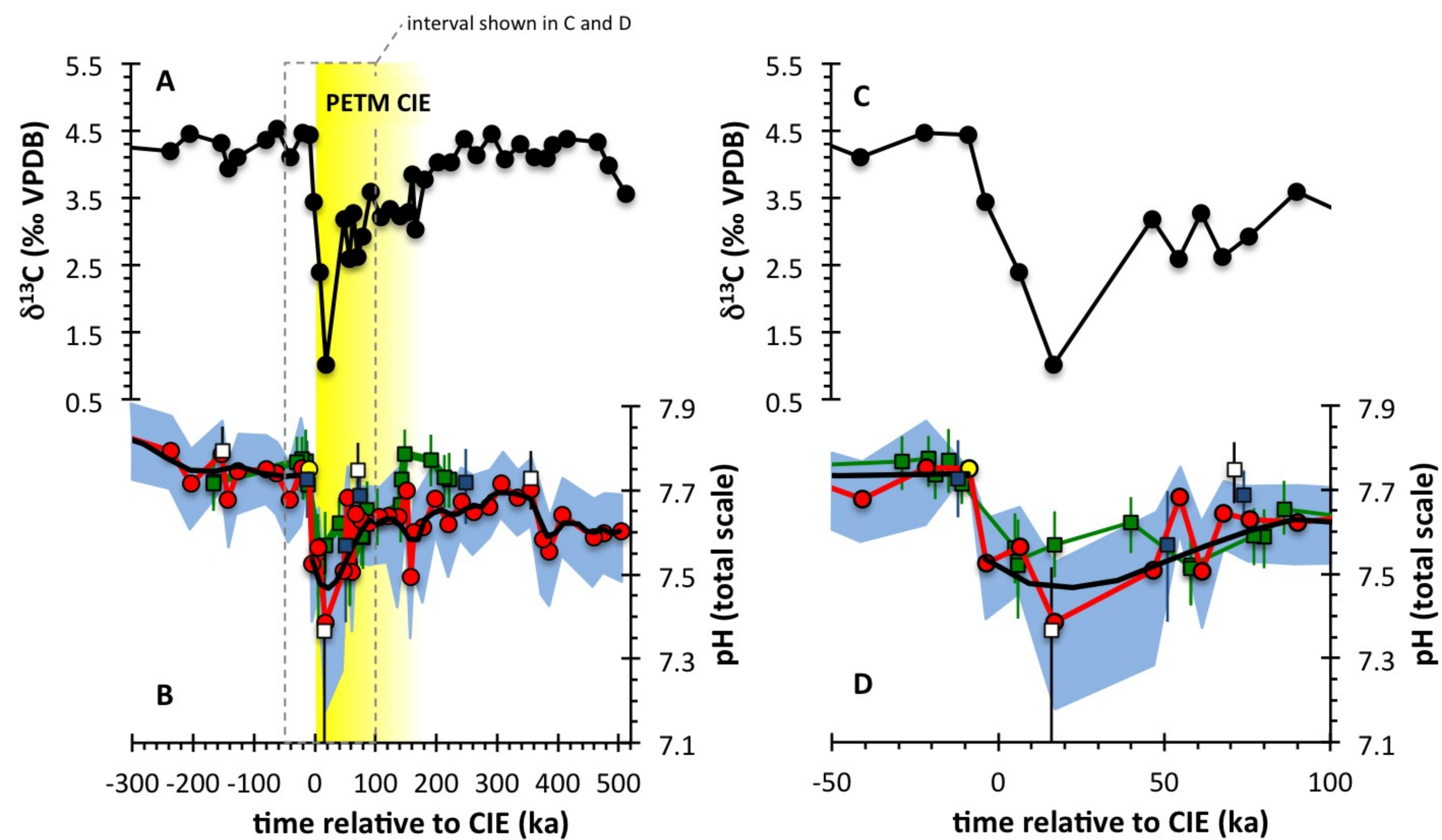
**Extended Data Fig. 9.** Down-core model-data evaluation at four data-rich sites. Shown are comparisons for four ocean drilling sites for which surface ocean pH has been reconstructed across the PETM (Fig. 2) – 401, 865, 1209, and 1263 (this study and ref. 24). Their paleo locations in the cGENIE Earth system model are shown to the side (panel q). Model-data comparisons are made for: (i) wt%  $\text{CaCO}_3$  (far LH panel for each site), (ii)  $\delta^{13}\text{C}$  of bulk carbonate (second-from-left series of panels), and (iii) surface ocean pH (third-from-left series of panels). To provide an orientation in time with regard to the evolution across the PETM event, the farthest-right series of panels shows the projected evolution of atmospheric  $\delta^{13}\text{C}$  of  $\text{CO}_2$  in the model. For wt%  $\text{CaCO}_3$  and  $\delta^{13}\text{C}$  of bulk carbonate, model points (resolved at 1 cm resolution) are plotted as filled yellow circles. Model-projected pH (global and annual mean, as per shown in Fig. 3j and Extended Data Fig. 6a) and atmospheric  $\delta^{13}\text{C}$  of  $\text{CO}_2$  are shown as continuous red lines. In all cases, observed data values are shown as stars (\*). The age models for Sites 865, 1209 and 1263 employing original relative age model constraints<sup>24</sup> used to convert from model-simulated sediment depth (resolved at 1 cm intervals) at each location in the cGENIE Earth system model, are calculated using a constant detrital flux accumulation rate. The observed data are plotting on

788 their respective site 690-derived age models<sup>29</sup>. Both model and data age scales are  
789 synchronized to age zero at PETM onset (horizontal line). See SI for details.

790 **Extended Data Table 1.** (a) Summary of the main double inversion experiments  
791 carried out. The terminology “R07” refers to configurations tying the Site 401 records  
792 to the chronostratigraphy of ref. 29, the notation “FE” refers to the <sup>3</sup>He-based age  
793 model of ref. 67). Annotation “sm” refers to inversion of analytically smoothed  $\delta^{13}\text{C}$   
794 and pH data sets, “rw” to usage of original sample data for double inversions. “HI”  
795 and “LO” represent potentially extreme configurations taking into account the boron  
796 proxy uncertainty at the 95% confidence level. “noW” has silicate (and carbonate)  
797 weathering feedbacks disabled. “Corg” denote model configurations that allow  
798 removal of excess organic carbon from the surface ocean. The outcome of “R07sm” is  
799 shown in Fig. 3a-f, that of “R07sm\_Corg” is illustrated in Fig. 3i-n. (b) Summary  
800 table presenting the results of sensitivity experiments (shown in Extended Data Fig. 5)  
801 designed to quantify the importance of uncertainties in the age model for the CIE  
802 onset. In these experiments, the CIE onset phase is assumed to occur linearly, with a  
803 duration of the decline in  $\delta^{13}\text{C}$  and pH that varies from 100 to 20,000 yr duration.  
804 Reported are: (1) the diagnosed peak carbon emissions (occurring at any time during  
805 the experiment), (2) the cumulative carbon emissions occurring over the duration of  
806 the onset, and the mean (flux weighted)  $\delta^{13}\text{C}$  of these emissions, (3) the cumulative  
807 carbon emissions occurring at the 20 kyr time horizon – comparable to the onset  
808 duration in our assumed age model, plus the mean (flux weighted)  $\delta^{13}\text{C}$  of these  
809 emissions, and (4) the cumulative carbon emissions occurring at the 20 kyr time  
810 horizon, which is the maximum model run duration in this series of experiments, plus  
811 the mean (flux weighted)  $\delta^{13}\text{C}$  of these emissions. Note that in all experiments, once  
812 the onset is complete, the target pH and  $\delta^{13}\text{C}$  values are held constant (and low) until  
813 the end of the experiment (50,000 yr).







● Site 401 (NE Atlantic)

□ Site 865 (Eq. Pacific)

— Site 401 (smoothed)

■ Site 1263 (SE Atlantic)

■ Site 1209 (N Pacific)



## Emissions only

Emissions + C<sub>org</sub> burial